

SH Waves, Rays, and Full Waveform Inversion

Laurence R. Lines, Edward S. Krebs and Patrick F. Daley

ABSTRACT

With the continuous advances in high performance computing and multicomponent seismic recording, there continues to be increased interest in full waveform inversion (FWI) of seismic data. The SH-wave mode is appealing since unlike P-wave and SV-wave modes, this seismic mode does not undergo mode conversions at a boundary. SH-waves have a viscoelastic reflection response that can be modeled by finite-difference modeling, ray tracing or analytic methods. Since these modeling methods could be used in the full waveform inversion of real shear-wave data, it is important to know the differences and similarities of these methods. For precritical arrivals, the finite-difference (FD) viscoelastic wave modeling agrees with the viscoelastic reflection coefficients from analytic expressions even though the 2-D FD method assumes a cylindrical wave source and the reflection coefficient expression is derived for plane wave reflections. It is shown that the plane waves can be constructed from a sum of cylindrical waves with varying time delays. Near the critical angle, the plane wave method breaks down, and the 2-D FD expression would seem to be favored. However, amplitudes for the 2-D FD method with cylindrical spreading does depart from the 2.5D hybrid method of Daley et al. (2009) which accounts for a point source undergoing 3-D spreading. For real data of recorded SH-waves, full waveform inversion should take into account these amplitude differences due to 3-D spreading when using FD models. Given these considerations and the need for methods that are computationally faster than 3-D finite-difference methods, it is recommended that the 2.5D hybrid scalar wave equation model be used for full waveform inversion of P-wave reflection data from flat interfaces.

INTRODUCTION

Within the family of elastic body waves, SH-waves are the least complicated in terms of mode conversions and boundary conversions. SH-waves are shear waves with only a horizontal displacement component normal to the propagation direction. They undergo no conversions to P-waves or SV-waves. In this paper, we model SH-wave reflections in viscoelastic media. This paper was inspired by a lecture by Dr. Krebs on SH-wave reflections entitled “Computing reflection coefficients in viscoelastic media”. We compare reflection strength from seismograms derived from finite-difference wave equation models to the reflection coefficients expected from analytic expressions. We contrast the reflections from cylindrical waves to the reflections from plane waves. The relationship between SH cylindrical waves from a line source and a point source is related to plane wave propagation. Ultimately, we discuss what SH-wave model may be appropriate for full waveform inversion of real data.

METHODOLOGY AND RESULTS

In order to understand SH-waves, it is instructive to consider a boundary between contrasting shear-wave velocities β_1 and β_2 as shown in Figure 1.

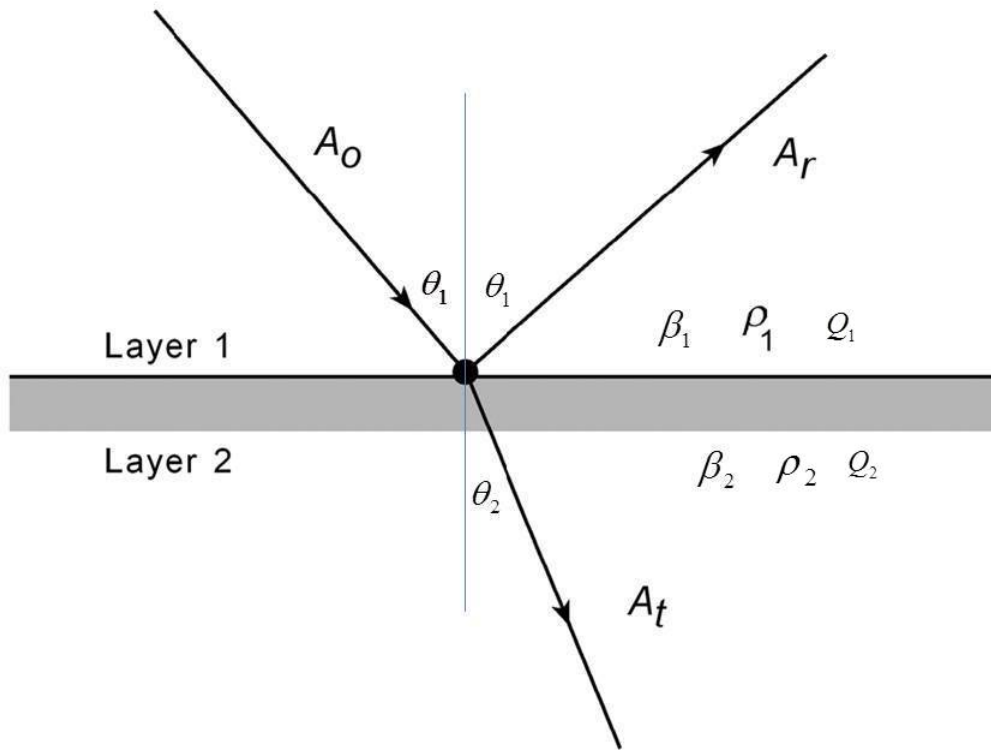


FIG. 1 The ray paths for the incident, reflected and transmitted SH waves for a two-layer model.

The ray paths for reflected and transmitted SH waves is essentially governed by Snell’s Law and the reflection coefficients are given by solutions to the boundary conditions. The wave nature of the propagation can generally be described by numerical solutions to the wave equation.

The incoming SH-wave has displacement normal to the sagittal plane. It undergoes no conversion to any other body wave, so in this sense, it is similar to the case of P-waves in a purely acoustical medium with fluid-filled layers. The rays undergo reflection and refraction according to Snell’s Law.

$$\frac{\sin\theta_1}{\beta_1} = \frac{\sin\theta_2}{\beta_2} = p. \quad (1)$$

Here p is the ray parameter representing horizontal slowness, given by:

$$p = \frac{\sin\theta_n}{\beta_n}, \quad (2)$$

and the fact that this is a constant for reflected and transmitted waves is a consequence of Snell’s Law.

Consider a quantity $\eta_n = \frac{\cos\theta_n}{\beta_n}$ which is the magnitude of the vertical slowness for the n th layer given by:

$$\eta_n = \frac{\cos \theta_n}{\beta_n} \quad . \quad (3)$$

The reflection coefficient for SH-waves, or the ratio of the reflected wave's displacement amplitude, A_r to the incident wave's displacement amplitude, A_0 for the wave in Figure 1 is shown by Krebs (1984) to be:

$$R_{SH} = \frac{A_r}{A_0} = \frac{\rho_1 \beta_1 \cos \theta_1 - \rho_2 \beta_2 \cos \theta_2}{\rho_1 \beta_1 \cos \theta_1 + \rho_2 \beta_2 \cos \theta_2} \quad . \quad (4)$$

The shear modulus for the nth layer is given in terms of density and shear-wave velocity by:

$$\mu_n = \rho_n \beta_n^2 \quad . \quad (5)$$

Using equations (3) and (5), we can write the SH-wave reflection coefficient in equation (4) as:

$$R_{SH} = \frac{\mu_1 \eta_1 - \mu_2 \eta_2}{\mu_1 \eta_1 + \mu_2 \eta_2} \quad . \quad (6)$$

The vertical slowness can be described in terms of the SH-wave velocity and the horizontal slowness by:

$$\eta_n = \sqrt{\frac{1}{\beta_n^2} - p^2} \quad . \quad (7)$$

In the purely elastic case with no attenuation, where the inverse quality factor, $Q^{-1} = 0$ or $Q = \infty$), all quantities in the above equations are real. In the viscoelastic case, Q is not infinite, the ray parameter becomes complex for the viscoelastic case (as shown by White (1965); Krebs and Hron (1980); and Lines et al. (2008)) is given by:

$$p = \frac{\sin \theta_l}{\beta_{l0}} \left(1 + \frac{i}{2Q_1} \right) \quad . \quad (8)$$

That is, the slowness for the elastic case is multiplied by a factor of $(1 + \frac{i}{2Q})$. The viscoelasticity causes a modification in the behaviour of the elastic case given by (4). Having considered ray paths from ray theory (which is a high frequency approximation to the wave equation) and reflection coefficients which are derived from boundary conditions that impose the continuity of displacement and stress, we now turn our attention to wave equation solutions for SH-waves.

The 2-D finite-difference (FD) solution to the wave equation for SH waves was given by Boore (1970) who solved the following SH-wave equation using finite-difference approximations to the second derivatives:

$$\rho \frac{\partial^2 v}{\partial t^2} = \mu \left[\frac{\partial^2 v}{\partial x^2} + \frac{\partial^2 v}{\partial z^2} \right] \quad . \quad (9)$$

Here ρ is the density of the rock layer, μ is the rigidity (shear modulus) and v is the horizontal displacement of the wave. In this paper, we compare and contrast the model responses for analytic viscoelastic reflection coefficients with FD viscoelastic solutions.

In comparing analytic and FD solutions, we use a simple 2-layer model defined by layer properties in the following table.

Table 1 – Properties of SH-wave model: density, velocity and Q value for SH waves.

Layer number	Density (gm/cc)	S-wave velocity (m/s)	Q
1	2.1	1000	15
2	2.2	2000	20

Figure 2 shows the geometry of an FD model with these velocity layers where the top layer has a thickness of 150 m. The dimensions of the model are 600 m in width and 600 m in depth. The source- receiver geometry for the model survey is given in Table 2. Source interval = 50 m and receiver interval = 5m. Source and receiver depths are both at 25 m.

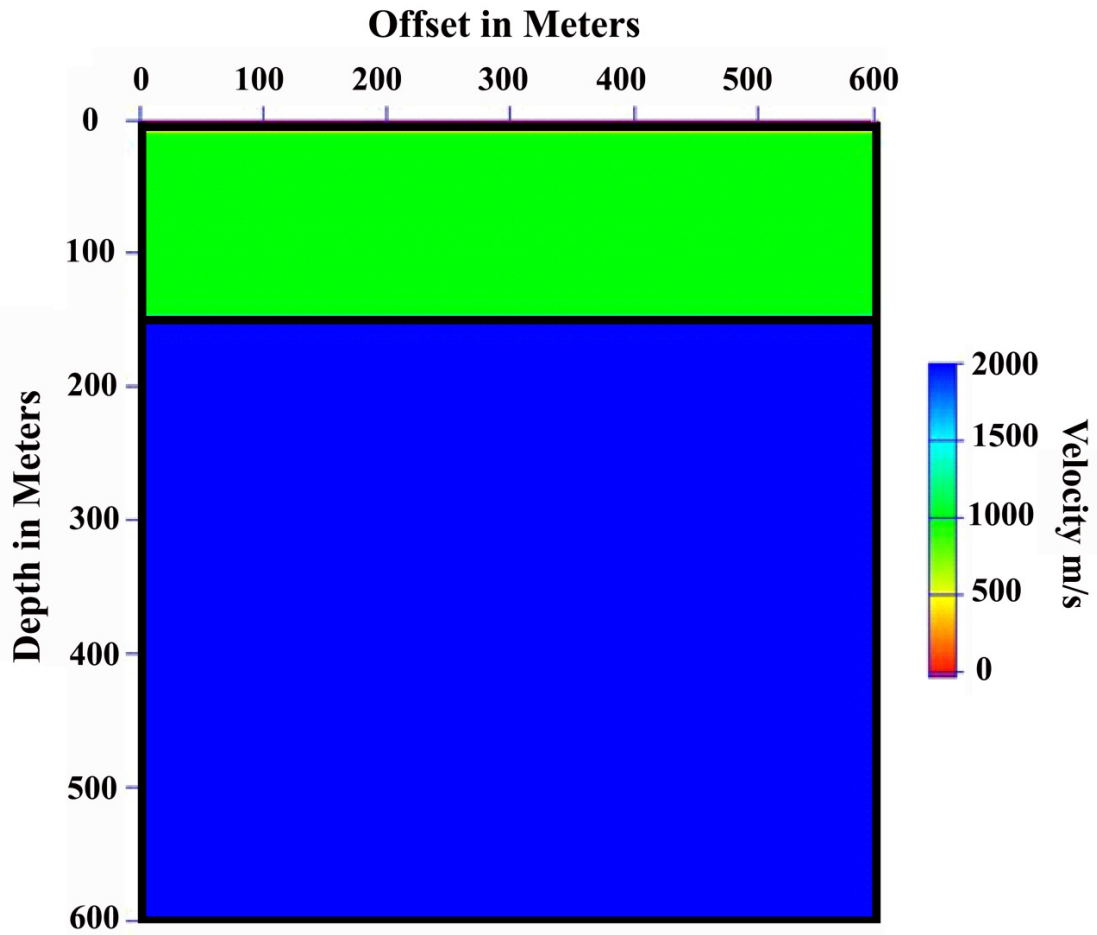


FIG. 2 Velocity model used for SH-wave modeling with properties in Table 1. FD model will have 120 rows and 120 columns with cell size=5m, giving dimensions of model as 600 m by 600m. Source-receiver geometry is given in Table 2 with source spacing = 10 cells or 50 m, source depth = 25m. Receivers at every grid point with spacing = 5m and receiver depth = 25m.

Table 2 – Source-receiver geometry and trace numbers for modeling acquisition

Source number	Source offset	Receiver locations	Trace number
1	95	0-595m	1-120
2	145	0-595m	121-240
3	195	0-595m	241-360
4	245	0-595m	361-480
5	295	0-595m	481-600
6	345	0-595m	601-720
7	395	0-595m	721--840
8	445	0-595m	841-960
9	495	0-595m	961-1080

In order to compare modeling results for SH-waves, we first compare the reflection coefficients for elastic and viscoelastic reflections. Such geometrical ray computations are similar to examples those shown by Krebs and Daley (2007). Figure 3 shows the reflection coefficients for our model contrasting the elastic case (red curve) and the viscoelastic (black curve).

In observing Figure 3, we note that for normal incidence where $p=0$, we anticipate a reflection coefficient given by 0.3538 and this is verified by the result in this figure. We also note that reflection strength does not appreciably change for precritical reflections from $p=0$ to $p=0.2$. Reflection strength decreases from $p=0.2$ to $p=0.45$ where it diminishes to 0 at $p=0.45$ before increasing to complete reflection (in the elastic case) at $p=0.5$. We note that the critical angle is $\sin^{-1}(1000/2000) = 30$ degrees. The ray parameter, $\frac{\sin(\theta)}{v} = 0.5$ ms/m for a velocity of 1000 m/s. From classical ray theory, it is anticipated that complete reflection occurs after the ray parameter exceeds the ray parameter for the critical angle. This is also verified by Figure 3 for the elastic case. We note that for the viscoelastic case, the reflection strength is diminished.

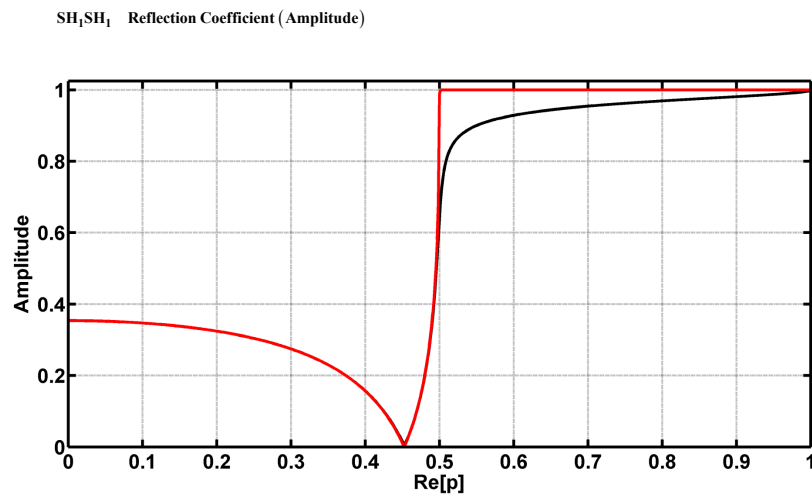


FIG. 3. SH-wave reflection coefficient as a function of ray parameter for the two-layer model in Figure 2. Red curve= elastic wave reflection coefficient; black curve=viscoelastic reflection coefficient. Critical angle at $\sin(\theta) = 0.5$ or $\theta = 30$ degrees, or ray parameter $p=0.5$.

We recall that the reflection coefficient calculations using geometric ray theory are computed for plane waves. We now switch our attention to FD calculations for a 2D model with a line source. The software used for these calculations is due to Carcione (2007). The theory for the FD solution to the SH-wave equation is also given by

Carcione (2007, p. 7, equation 1.46). If σ_{ij} represents the stress tensor, in a 2-D medium with layers in the x-z plane and no variation in the y direction, the SH-wave is only influenced by stress components σ_{12} and σ_{23} . SH-wave displacement motion is only in the y (ie x_2 direction) denoted by u_2 . If we designate $v_2 = \frac{\partial u_2}{\partial t}$ as the velocity of the horizontal displacement in the y direction, we obtain the equation of motion as

$$\rho \frac{\partial v_2}{\partial t} = \frac{\partial \sigma_{12}}{\partial x_1} + \frac{\partial \sigma_{23}}{\partial x_3} + f_2 \quad , \quad (6)$$

where f_2 is an external force in the x_2 direction.

The viscoelastic stress-strain relationships for the SH-wave in an isotropic medium yields the following:

$$\frac{\partial \sigma_{23}}{\partial t} = \mu \frac{\partial v_2}{\partial x_3} \quad (7a)$$

$$\frac{\partial \sigma_{12}}{\partial t} = \mu \frac{\partial v_2}{\partial x_1} \quad . \quad (7b)$$

Equations (7a) and (7b) are essentially the time derivatives of Hooke's Law relationship between shear stress and shear strain for an isotropic medium. Equations (6), (7a), and (7b) are the same as equation (1.46) from Carcione (2007) for the isotropic case where elasticity constant $c_{46} = 0$. The finite-differencing of the wave equation resulting from equations (6), (7a), 7(b) allowed Carcione (2007) to compute solutions for SH waves in a viscoelastic isotropic medium. Carcione's code was used to compute wave equation solutions for our model.

Figure 4 shows a seismogram for a shot placed near the middle of the model. This seismogram is for shot #5 as listed in Table 2. The seismogram is recorded by each of 120 receivers at the surface at each grid point, each with 5 m separation and the shot gather dominated by the direct arrival and reflection arrivals. In order to emphasize the reflected arrivals, we will effectively remove the direct arrivals to produce the reflection seismogram of Figure 4.

In observing the reflection amplitudes of Figure 4, we note a significant change in amplitudes at receiver offsets of about 30 grid points (150 m) from the centre of the model on each side of station 59 This will correspond to the offset at which rays reach the critical angle. For a velocity in layer 1 of 1000 m/s and a velocity in layer 2 of 2000 m/s, the critical angle is $\sin^{-1}(1000/2000) = 30$ degrees. This corresponds to a tan value of 0.58 for $(x/2)/z$, where $x/2$ is the horizontal offset of the reflected ray and z is the depth of the reflector beneath the source-receiver depths. In other words, critical reflections occur when $x=2z \tan(30 \text{ degrees})$. Since $z = 125\text{m}$ (25 grid points), we have $x=2(125)(0,58) = 145 \text{ m}$, which is 29 grid points from source to receiver. Critical reflections will occur at stations 30 and 88 in Figure 4. Significant amplitude changes are seen in this area.

In analyzing the strength of reflected arrivals, it is often useful to compute the trace envelope seismogram. As shown by Clayton et al. (1976), trace envelopes are insensitive to phase shifted arrivals in the seismogram. The envelope is essentially determined by the amplitude of the analytic signal. In order to compare amplitudes of traces, the envelopes of the traces in Figure 4 are computed and displayed in Figure 5. In order to compare trace-to-trace amplitudes, we compute the maximum value of the envelopes for the reflected arrivals. For pre-critical reflections, these amplitudes show a great similarity to reflection amplitudes from geometric ray theory.

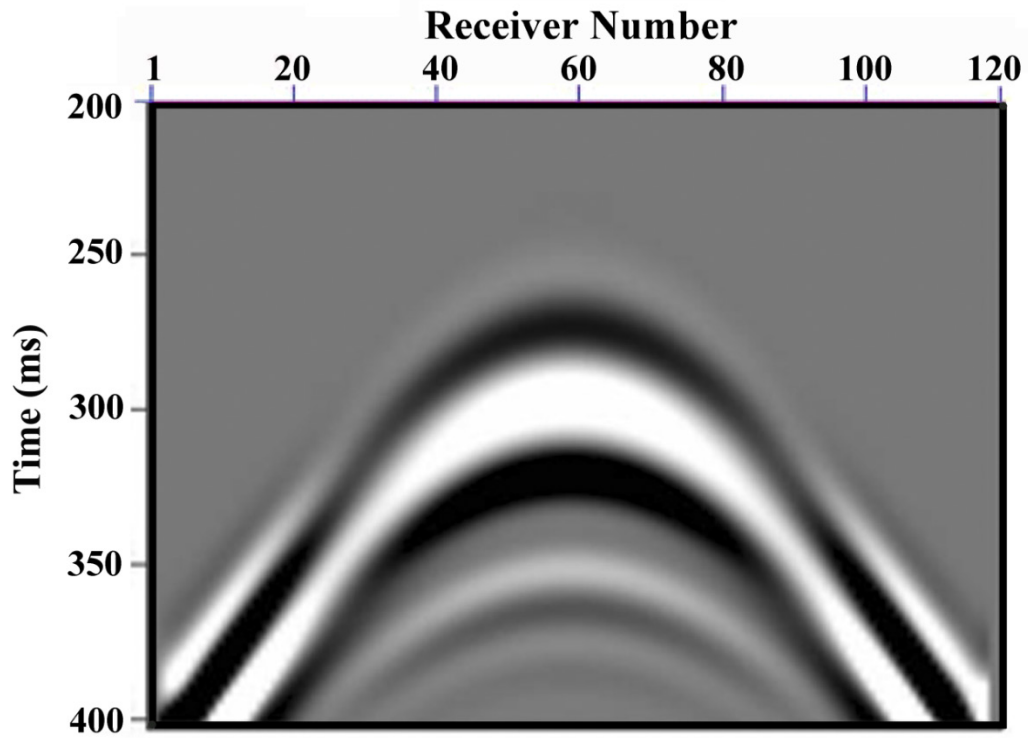


FIG. 4 The reflection response for the 2-layer model after removal of the direct wave .

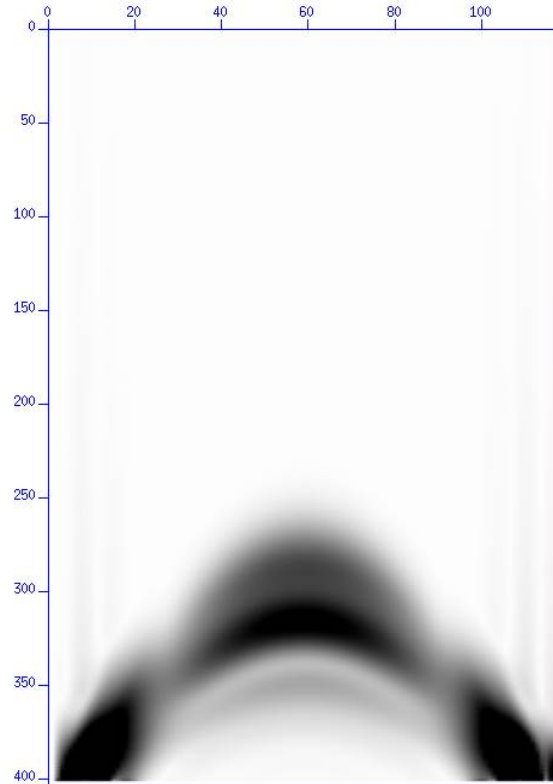


FIG. 5. The trace envelopes for the seismic record in Figure 4.

A comparison of FD wave amplitudes with the analytic computations is shown by Figure 6 where the envelope maxima are overplotted (with blue stars) to compare to the ray synthetic amplitudes from Figure 3. For the precritical reflections, the FD wave equation amplitudes are very similar to the behaviour predicted by ray synthetic modeling. As the critical angle is approached, amplitudes decrease for both the FD wave equation calculations and ray synthetics. Unlike the ray synthetics, the FD wave equation amplitudes never completely vanish. This is because the wave equation stars show the ``generalized reflection response`` or exact response for a line source of cylindrical waves, whereas the black and red curves show the plane wave reflections which are used in ray theory. For postcritical arrivals, the FD reflection amplitudes increase but are not as big as the ray synthetic amplitudes. The answer to this may come in realizing that ray synthetics model plane waves while the 2D FD synthetics model cylindrical waves from a line source. These issues are addressed in a later section.

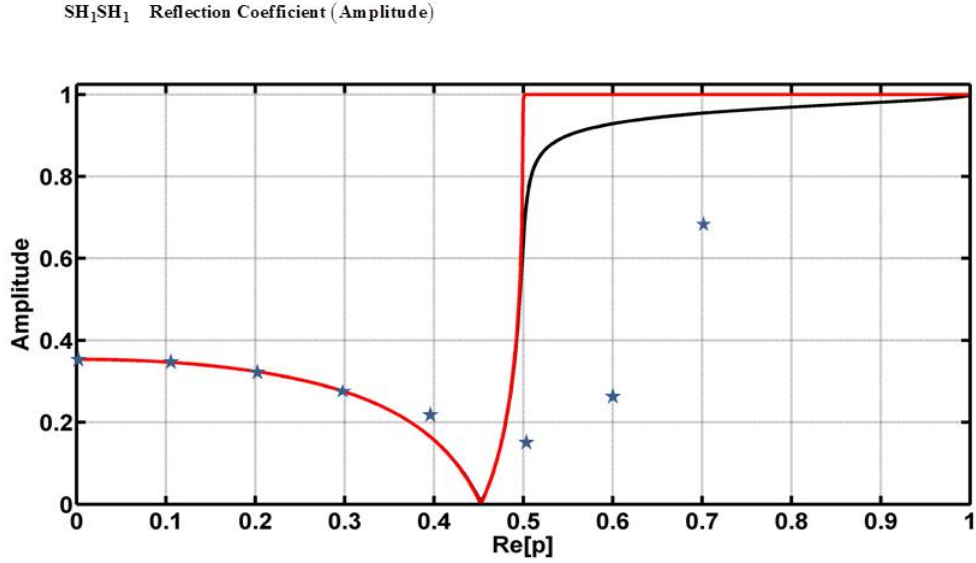


FIG. 6. A comparison of the SH reflection coefficients (Figure 3) for the elastic (red curve) and viscoelastic (black) curves with the maxima of trace envelopes for the FD synthetic seismogram (blue stars) for ray parameters corresponding to different source-receiver offsets. For small angle precritical reflections, the reflection strengths are similar for the ray and wave calculations. Near the critical angle ($p=0.5$), the curves diverge. Past the critical angle, the ray synthetics give complete reflection (in the elastic case) or nearly complete reflection (viscoelastic case) while the FD wave amplitudes show less of an increase.

Seismic recordings in exploration seismology are generated by dynamite explosions that can be considered as point sources (in the case of localized charges in a 3-D model) or as line sources (in the case of distributed charges extended in the strike direction). For 2-D models, these wave fronts will appear to be circular in a medium of uniform velocity. At great distances from the source, these wave fronts may be approximated by plane waves in a far-field approximation.

The simulation of plane waves by summation of cylindrical waves has been described by Sommerfeld (1964) and a plane wave function can be mathematically described as a sum of Hankel/Bessel functions.

According to Sommerfeld, the plane wave expansion in cylindrical coordinates (r, θ, z) can be written as:

$$e^{ik \cdot \mathbf{r}} = \sum_{n=-\infty}^{\infty} i^n J_n(z) e^{in\theta}. \quad (8)$$

Here $e^{ik \cdot r}$ represents the spatial variation of a plane wave and $J_n(z)$ is an n th order Bessel function. In other words, the plane wave can be represented as an infinite sum of circular waves. While plane waves are generally considered to be non-physical since they are infinite in extent, they can be approximated by a summation of cylindrical waves.

Alternatively, we can consider a spherical wave from a point source as a weighted sum of plane waves in the Sommerfeld integral expansion (Aki and Richards, 1980, p. 199). This process known as plane wave decomposition is described by Treitel et al. (1982).

In exploring the appropriate models for seismic data, we do some simple computational experiments to relate plane waves to cylindrical waves or spherical waves. For our 2-D model example, we compute a sum of seismograms for the cylindrical waves from the FD solutions to produce approximations to plane waves.

This numerical simulation has actually been done in field tests in which a series of seismic shots are exploded simultaneously. An Amoco experiment, in Figure 7 taken from Whitmore (1995), shows the explosion of a number of dynamite shots to create a series of downgoing wavefronts. The summation of these seismic wavefronts will create a downgoing plane wave, as shown in the lower part of Figure 7.

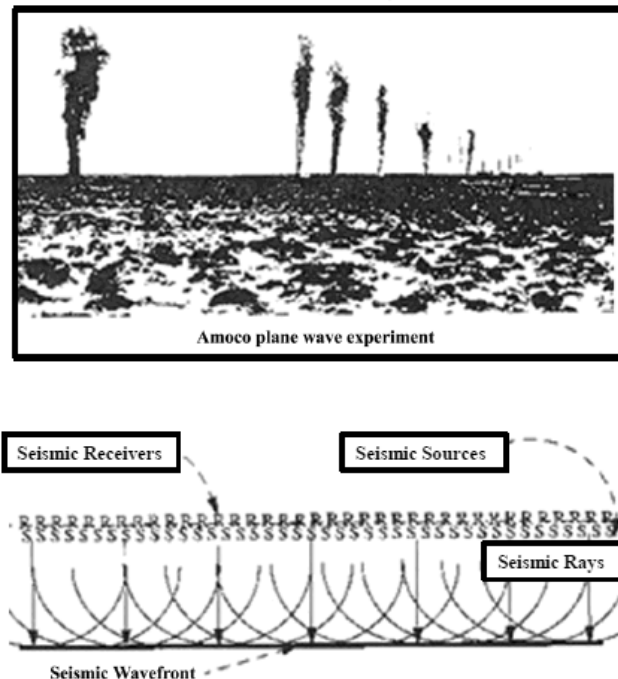


FIG 7. The Amoco plane wave experiment, as described by Whitmore (1995). A plane wave can be constructed by the superposition of wavefronts. The direction of the wavefront can be controlled by time delays for the sources.

In the case where there is no time delay between the shots in a uniform medium, the resulting plane wave travels vertically downward, as shown in Figure 7. A plane wave record can be simulated at different angles by delaying the shot records and summing.

We can numerically simulate the normally incident plane wave by summation of the circular wave fronts. Figure 8 shows the wavefronts for wave propagation through our model.

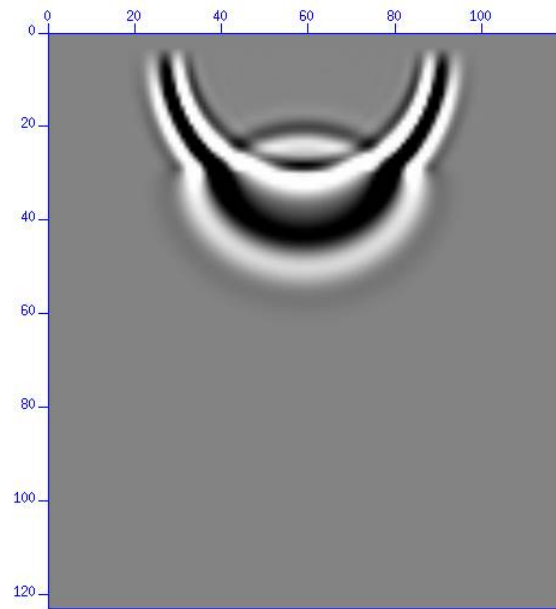


FIG 8. shows the wavefronts for the 201st time step of wave propagation through model 2.

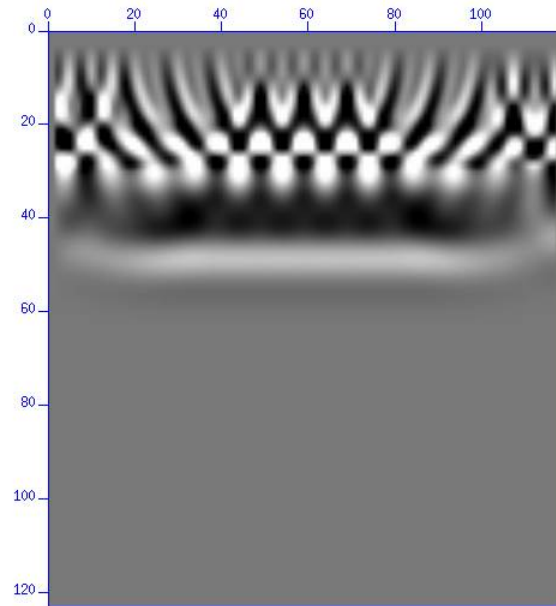


FIG. 9. Sequence of wavefronts obtained by initiating 9 shots placed at positions described in Table 2. Note the the constructive interference on the leading edge of the wave front approximates a plane wave propagating vertically downward.

If we place shots according to the positions described in Table 2, we obtain a series of nine 120-trace records as shown in Figure 10. The reflection records for these 9 shots, shown in Figure 11, is obtained by subtracting off the direct arrivals.

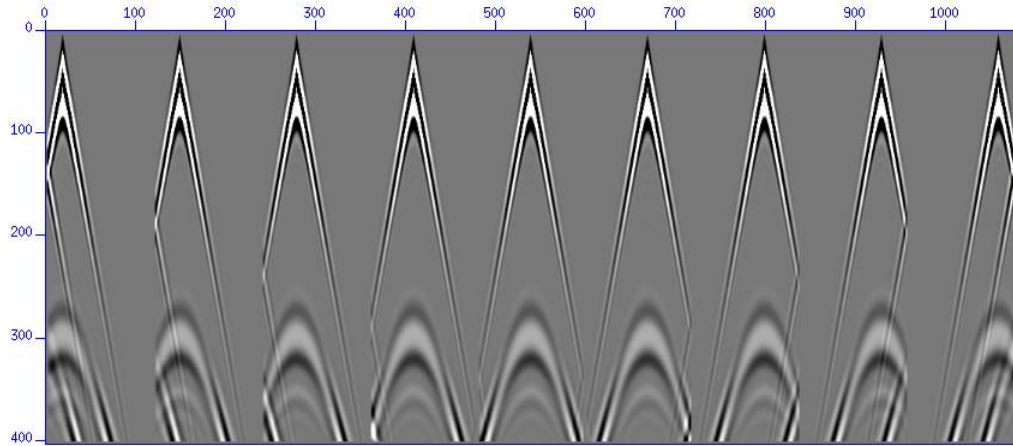


FIG. 10. The sequence of 1080 traces for all 9 shots described in Table 2. The first 120 traces are for the shot at $x=95\text{m}$. Each subsequent shot record of 120 traces is for a shot at 50 m spacing from the previous shot. 120 Receivers are spaced 5m apart at every grid point.

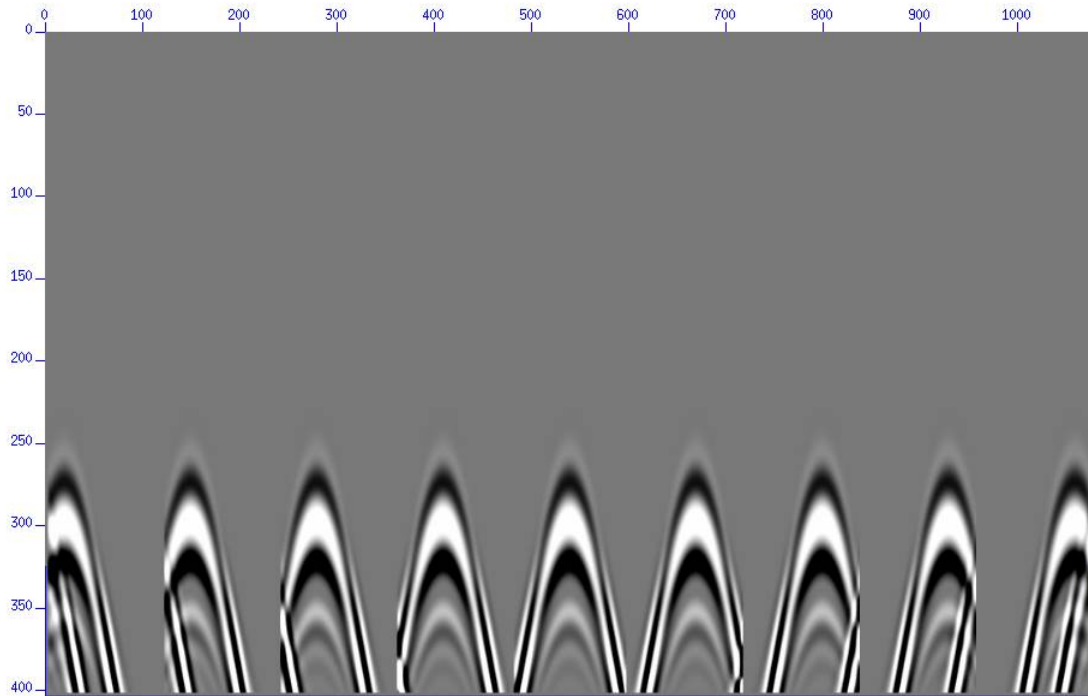


FIG 11. Sequence of 9 shot records for the reflection responses for the traces of Figure 10 obtained by subtracting off direct arrivals and rescaling.

If we sum the sequence of shot records shown in Figure 11 we obtain an approximation of the reflected record for a downgoing normally incident plane wave in Figure 12. The leading edge of this reflection is a good simulation of a plane wave reflector. The simulation will improve if we add more shot records. If we use a window of 80 ms - about the length of the source wavelet, we obtain a good reflection record for a normally incident plane wave as shown in Figure 13.

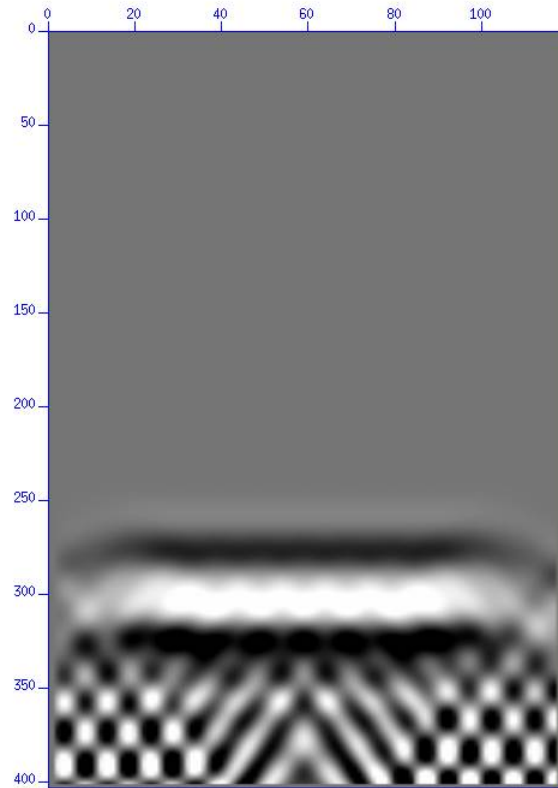


FIG 12. The summation of wave fronts resulting from the summation of the 1080 traces in Figure 11 results in a reflected plane wave simulation for a downgoing plane wave..

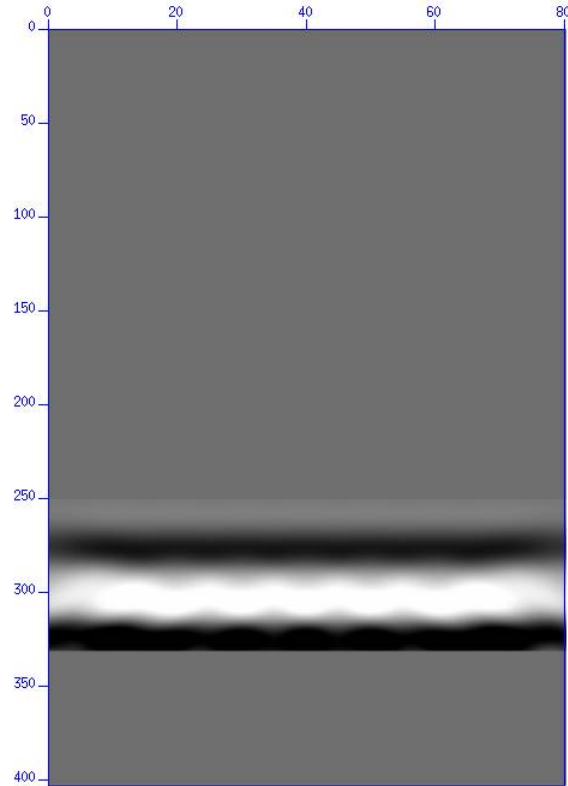


FIG. 13. A window of 80 ms for the trace summation in Figure 12 results in a reflected wave that closely approximates a plane wave at normal incidence.

If we wish to simulate a plane wave at an angle, we can simply delay the shot records and sum. From equation (2) the ray parameter is given by $p = \frac{\sin \theta_n}{\beta_n}$. If one wave is delayed from another by an amount Δt , and the sin of the emergent angle is $\sin \theta = \frac{\beta_0 \Delta t}{\Delta x}$, where Δx is the spacing between receivers, then the time delay for a plane wave for a ray parameter p is given by: $\Delta t = p \Delta x$. Figure 14 shows the plane wave simulations for $p=0$ and $p=0.1$ ms/m.

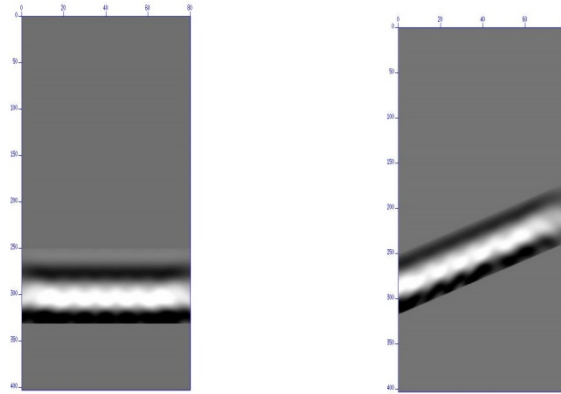


FIG. 14. Plane waves at different angles can be simulated by delaying and summing the circular wave fronts from FD calculations. Left hand seismicogram is for $p=0$ and right hand seismicogram is for $p=0.1$ m/ms.

Figures 13 and 14 show approximations to plane wave propagation by summing shot gathers. The plane wave approximation will improve as we sum more shot gathers. For FD computations, the ultimate summation would be to use a shot at every grid point. There is a very efficient way to do this (at least for flat reflectors) and that is to propagate a reflected wave upward 1-way to the receivers using a source at every point on the reflector at $\frac{1}{2}$ the true velocity. This is the exploding reflector model. From Figure 15 we see that this use of the exploding reflector model produces an excellent model of a plane wave at normal incidence at very low cost.

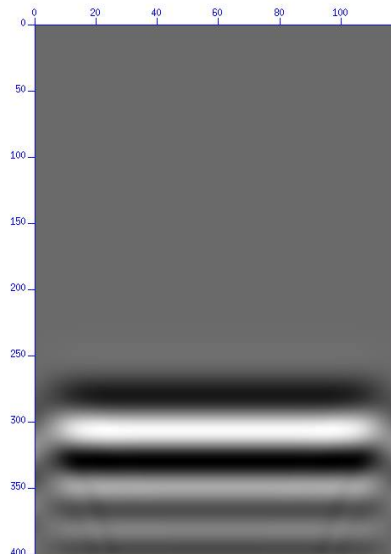


FIG. 15 Simulation of a normal incidence plane wave similar to Figure 15 by use of the exploding reflector model.

We see that while the 2-D FD synthetic modeling computes seismic responses for cylindrical waves in a 3-D world, the ray synthetics are computed for plane waves. By use of Sommerfeld's analysis, we know that these wave/ray models are related. We can approximate plane waves through the summation of cylindrical waves (or spherical waves in 3-D). Alternatively, we can consider cylindrical wave fronts to be an infinite sum of plane waves. This analysis is analogous to Fourier transforms where we can consider a signal in time to be composed of an infinite sum of sinusoids. The question arises. For the real world, what model do we use? This is especially crucial for full waveform inversion.

CONCLUSIONS

In full waveform inversion of SH-waves we hope to match model responses to real data. The models considered in this study were 2-D FD wave equation simulations and ray synthetics. While these SH-wave model responses are similar for small angles in precritical reflections, there are differences related to circular wave fronts and plane waves especially at near-critical or post-critical reflections.

In terms of models that match real wave propagation, it would seem that 3-D FD calculations of SH-wave propagation is appropriate. For flat layers, one might be tempted to use the 2-D FD models shown here. However, for seismic modeling of amplitude variation with offset for flat layers in a 3-D world (a 2.5 D model), one cannot ignore the differences in wave propagation spreading effects between 2-D cylindrical wavefronts and 3-D spherical wavefronts in a 2-D model. These differences between 2-D and 2.5D solutions, are shown by Daley et al. (2008). It would appear the 2.5 D finite-difference solutions to the SH-wave equations might prove to be the answer for full waveform inversion, but further research is warranted for at least three reasons. First, Daley et al. (2008) show that there are significant amplitude differences between 2-D and 2.5 D (while the traveltimes differences between the traces is a small static shift). Secondly, the 2.5D amplitudes are nearly identical to those obtained by 3-D finite-difference modeling (Novais and Santos, 2005) for flat layer models. Thirdly, the computational run times are substantially less for the hybrid Fourier Transform/ finite difference 2.5D calculations than for the 3-D finite-difference calculations.

The choice of an appropriate model for full waveform inversion would be dependent on the nature of the actual geology and the source-receiver offsets in the data. For near-offset and precritical angles that are less than half of the critical angle, ray reflectivity and wave models are very similar. For visco-elastic materials, the visco-elastic reflectivity computations need to be made. In the far-field at small offset, the finite-difference wave equation solutions can be approximated by plane waves. In the case of reflections at angles near the critical angles, wave equation amplitudes are needed. In the case of flat-layer geology, 2-D, or better yet 2.5D wave equation solutions, are appropriate. For cases of complex geology with significant 3-D variation, the 3-D finite-difference computations will be needed for accuracy, but such calculations may be prohibitively expensive for full waveform inversion unless the initial guess is very close to the correct answer.

ACKNOWLEDGEMENTS

We thank the sponsors of this research including the Consortium for Research in Elastic Wave Exploration Seismology (CREWES), Consortium for Heavy Oil Research by University Scientists (CHORUS) and the Natural Science and Engineering Research Council of Canada (NSERC). We also thank Dr. Sven Treitel of Tri-Dekon Inc. for his constructive comments, questions and suggestions that have improved this paper.

REFERENCES

- Aki, K., and Richards, P., 1980, Quantitative seismology, W.H. Freeman and Company, San Francisco, Ca.
- Boore, D.M., 1970, Finite-difference solutions to the equations of elastic waves propagation with applications to Love waves over dipping interfaces, Ph.D. thesis, Massachusetts Institute of Technology.
- Carcione, J., 2007, Wavefields in real media: Elsevier Publishing Co., ISBN-13 978-0-08-046408-4.
- Clayton, R.W., McClary, B., and Wiggins, R.A., 1976, Comments on the Paper: "Phase distortion and Hilbert transformation in multiply reflected and refracted body waves, Bulletin of the Seismological Society of America, 66, no.1, 325-352.
- Daley, P.F., Krebes, E.S., and Lines, L.R., 2008, A hybrid method applied to a 2.5D scalar wave equation, *Can. J. Earth Sci.*, 45, 1517-1525.
- Krebes, E.S., and Hron, F., 1980, Ray-synthetic seismograms for SH waves in anelastic media, *Bulletin of the Seismological Society of America*, v. 70, no. 1, 29-46.
- Krebes, E.S., 1984, On the reflection and transmission of viscoelastic waves – Some numerical results, *Geophysics*, 49, 1374-1380.
- Krebes, E.S., and Daley, 2007, Difficulties with computing anelastic plane-wave reflection and transmission coefficients, *Geophys. J. Int.*, 170, 205-216.
- Lines, L., Vasheghani, F. and Treitel, S., 2008, Reflections on Q. *CSEG Recorder*, December, 36-38.
- Novais, A., and Santos, L.T., 2005, 2.5D finite-difference solution of the acoustic wave equation, *Geophysical Prospecting*, 53, 523-531.
- Lines, L., Vasheghani, F. and Treitel, S., 2008, Reflections on Q. *CSEG Recorder*, December, 36-38.
- Sommerfeld, A., 1964, *Partial differential equations in physics*, Academic Press, New York, NY.
- Treitel, S., Gutowski, P.R., and Wagner, D.E., 1982, Plane wave decomposition of seismograms, *Geophysics*, 47, 1375-1401.
- White, J.E., 1965, Reflections from lossy media. *The Journal of the Acoustical Society of America*, 38, 604-607.
- Whitmore, N.D., 1995, An imaging hierarchy for common-angle plane wave seismograms, Ph.D. thesis, University of Tulsa.